Opt Quant Electron (2017) 49:35
DOI 10.1007/s11082-016-0868-4

Efficient generation of a continuous-wave, tunable 780 nm laser via an optimized cavity-enhanced frequency doubling of 1.56 μm at low pump powers

Shanlong Guo[1] · Junmin Wang[2]

Received: 25 August 2016 / Accepted: 20 December 2016 / Published online: 3 January 2017
© Springer Science+Business Media New York 2016

Abstract We present the strict design parameters of the experiment for the 780 nm tunable continuous-wave second harmonic (SH) generation by the nonlinear resonator containing a MgO doped periodically poled $LiNbO_3$ (MgO:PPLN) crystal. Optimization of such critical parameters, including focusing and impedance matching, more than 84% SH conversion efficiency and 3.1 W available output power at 780 nm were obtained from the fundamental wave at 1560 nm with two different input couplers. The thermal saturated behavior of the SH output power has been observed in the experiment. The beam quality factor M^2 of the generated SH wave is 1.04 (1.03), and the RMS power stability is 1.29% in 3 h. The SH wave was further used to detect the D_2 transitions of Rb atom, exhibiting a fine tunable characteristic. Such laser source can be a suitable candidate in the atomic physics and quantum optics.

Keywords Second harmonic generation · 780 nm laser · Cavity-enhanced configuration · Rubidium atoms · MOPA

1 Introduction

High power, good beam quality and frequency tunable 780 nm continuous-wave (CW) laser has attracted huge attentions as it corresponds to the rubidium (Rb) D_2 line. There are many applications in the fields of atomic physics, spectroscopy and quantum optics. For atom storage systems, the 780 nm laser is naturally suitable for the long-lived Rb atomic memory (Hétet et al. 2008). If the ^{87}Rb magneto-optical trap (MOT) is taken as the storage medium, the high-power trapping and cooling laser at 780 nm will be helpful to achieve a

✉ Shanlong Guo
guoshanlong@vip.qq.com

1 Department of Physics, College of Applied Science, Taiyuan University of Science and Technology, Taiyuan 030024, People's Republic of China

2 State Key Laboratory of Quantum Optics and Quantum Optics Devices, Institute of Opto-Electronics, Shanxi University, Taiyuan 030006, People's Republic of China

large optical depth in quantum storage applications (Sparkes et al. 2013). Two-color continuous variable entangled optical beams at 780 and 1560 nm can be the potential quantum entangled sources used to the long-distance quantum communication (Chanelière et al. 2006; Guo et al. 2012).

Recently, a great deal of effort has focused on the development of high power, good beam quality CW sources at 780 nm. The frequency tunable Ti:sapphire laser covers a wide wavelength range, and the output power can be achieved >1 W at 780 nm. The commercial tapered diode lasers can also directly provide Watt-level power at 780 nm, but the beam quality is typically poor ($M^2 < 1.5$). Spatial filtering with a fiber can improve the beam quality; however, it results a reduction of the output power (<500 mW).

Thanks to the rapid development of high power fiber lasers and master-oscillator power amplifier (MOPA) laser systems at 1560 nm (Yang et al. 2013), an alternative solution to obtain the 780 nm laser source has been provided by using nonlinear crystal $\chi^{(2)}$ effect. Sané et al. (2012) used the fiber lasers frequency-doubled system with a periodically poled lithium niobate (PPLN) crystal to give 11 W output power at 780 nm via a single-pass configuration. Dingjan et al. (2006) employed the MOPA at 1560 nm to amplify pulsed seed laser and generated a peak power up to 12 W of 780 nm laser by the single-pass frequency doubling in the PPLN crystal.

The single-pass configuration is a simple way to give high second harmonic (SH) output power (Sané et al.2012; Henderson et al. 2010; Chiow et al. 2012; Thompson et al. 2003; Samanta et al. 2010; Zeil et al. 2013; Kobayashi et al. 2016), but a higher fundamental wave (FW) input power (>5 W) is generally needed. At low pump powers ($\leq$5 W), the SH conversion efficiency is obviously hampered by the low nonlinear gain of the nonlinear crystal. To improve the SH conversion efficiency at low pump powers, the cavity-enhanced configuration has been deployed (Ou et al. 1992; Khripunov et al. 2014, 2016; Wen et al. 2014; Targat et al. 2005). Feng et al. (2007) demonstrated a 670 mW CW single-frequency laser source at 780 nm by using cavity-enhanced SH generation at the pump power of 1.28 W, and the maximum SH conversion efficiency was 58%. Hayasaka et al. (2004) reported the frequency doubling of an extended-cavity diode laser, which generated green laser at 540 nm of 22.8 mW from a FW input power of 44.2 mW. Hou et al. (2016) reached a power of 742 mW laser at 780 nm through an extra-cavity frequency-doubled system with an input power of 1.41 W, corresponding to the SH conversion efficiency of 52.6%. Jensen and Petersen (2013) presented more than 500 mW SH output power of the diffraction limited green light by using a coupled ring cavity, and the optical conversion efficiency exceeded 30%. Ast et al. (2011) reported a SH power of 1.05 W at 775 nm in a nonlinear cavity, yielding a total external conversion efficiency of 95%. Eismann et al. (2013) obtained 2.1 W intra-cavity frequency-doubled single-frequency lasers at 671 nm with a nonlinear conversion efficiency of 88%. Li et al. (2015) used a standing-wave cavity to reach the SH conversion efficiency of 50% with an input power of 60 mW at 1064 nm. In our early work, the SH output power of 1.5 W at 780 nm has been realized from a cavity-enhanced frequency doubling of 1560 nm MOPA (Ge et al. 2015); however, a further improvement of the SH output power was limited by the cavity length design, the linear loss and the impedance matching of the cavity. Some useful advices on improving the SH conversion efficiency have been given in the previous papers (Ou et al. 1992; Ge et al. 2015), but the corresponding experimental results have not yet been seen. The purpose of our work is to extend the investigations of the cavity-enhanced SH experiment to achieve the continuous frequency tuning and the higher output power of 780 nm laser at low pump powers, which can be served to the physical experiment working with Rb atom. Although the cavity-enhanced frequency doubling technique is common, the optimizations of such schemes are not trivial. The analyses of the optimizations of the cavity-enhanced configuration will be helpful to the related SH experimental work.

Basically, the direct factor related to the improvement of SH conversion efficiency of the cavity-enhanced configuration is the FW circulating power in the resonator. There are two primary considerations. One is the mode matching of the resonator. The mode matching can achieve the maximum overlap between the FW mode volume and the cavity mode volume. The mode matching can be a good performance by using the lens group in the experiment. A second is the impedance matching of the resonator. The impedance matching will couple more FW power, which involved in the SH conversion process, into the resonator. It means choosing the suitable transmission of the input coupler of the resonator. Additionally, the lower linear loss is helpful to provide the higher SH conversion efficiency. The semi-monolithic and monolithic cavity configurations were designed for this purpose (Deng et al. 2013; Wang et al. 2016; Paschotta et al. 1994). The linear loss includes the residual reflection of the antireflection surfaces, residual transmission of the high-reflection cavity mirrors and the absorption of the crystal, but it do not contain the transmission of the input coupler.

In this paper, we present the vital parameter designs of the four-mirror bow-tie ring resonator used to the frequency doubling of 1560 nm laser. Based on the optimum designs, we obtained a maximum SH output power of 1.96 W and 3.1 W at 780 nm with two different input couplings (11.0% and 25.5%) of the resonator, respectively. The corresponding maximum SH conversion efficiencies were 84.2 and 68.2%. The thermal induced saturated behaviors of the SH output power have been observed in the experiment. The beam quality factor M^2 of the generated SH wave is 1.04 (1.03), and the RMS power stability is 1.29% in 3 h. We also successfully used this 780 nm SH source to pump a three-mirror sum-frequency generation cavity (Guo et al. 2015).

2 Experimental setup

The schematic of experimental setup is shown in Fig. 1. The CW seed light was from a 1560 nm external cavity diode laser (ECDL) in the Littman configuration (Newfous TLB-6328). The seed light was taken as the FW after being amplified by a commercial 5-W Er-doped fiber amplifier (EDFA). A half-wave plate was used to adjust the polarization of FW. In order to achieve a good mode matching of the four-mirror ring resonator, instead of single lens, the lens group was used in the experiment (L1 with a focal length of 500 mm, L2 with a focal length of 300 mm). The resonator consisted of two plane mirrors (M1 and M2) and two concave mirrors with a radius of 100 mm (M3 and M4), and the beam waist of the resonator was 39 μm inside the nonlinear crystal. The cavity mirrors M2–M4 were coated for high reflectivity at 1560 ($R > 99.8\%$) while M4 was high transmission at 780 nm ($T = 98.0\%$). The cavity mirror M1 was partly transmission at 1560 nm, and there were two optional input coupling mirrors used in our experiment (11.0 and 25.5%). To reduce the linear loss of the resonator effectively, all the cavity mirrors were super polished with high-quality optical film. The PZT was stuck on the M2 for scanning and stabilizing the cavity length. The dither-locking method was used to stabilize the cavity length to the FW resonant peak.

The nonlinear crystal was 5 mol.% MgO doped PPLN (MgO:PPLN) crystal (HC photonics Corp.). It had the dimension of $1 \times 3.4 \times 25\ \mathrm{mm}^3$ with the quasi-phase-matched (QPM) period of $\Lambda = 19.48$ μm. Both facet surfaces of the MgO:PPLN crystal were

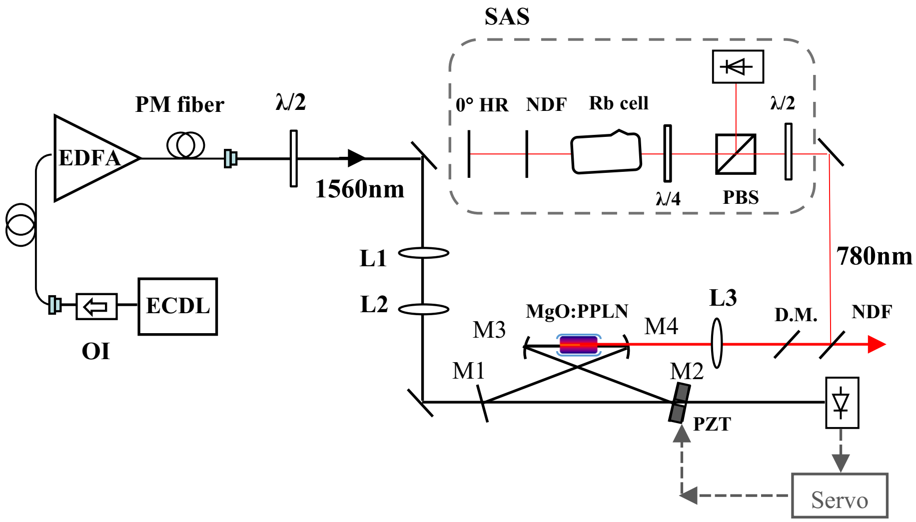

Fig. 1 The schematic diagram of the experimental setup. *OI*. optical isolator, *PM fiber* polarization maintaining fiber, *λ/2* half-wave plate, *λ/4* quarter-wave plate, *L1, L2* mode matching lens group, *L3* collimating lens, *M1–M4* cavity mirrors, *D. M.* dichroic mirror, *NDF* neutral densities filter. The *dash line* is the electronic servo loop used to lock the cavity length

anti-reflection coated for the FW and SH wave ($R_{1560nm\&780nm} < 0.05\%$). The crystal was mounted in a homemade copper oven with a temperature stability of ±0.01 °C. The absorption coefficients of the MgO:PPLN for both wavelengths are $\alpha_{1560} < 0.1\%/cm$ and $\alpha_{780} < 0.1\%/cm$, respectively.

The SH wave was separated from the FW by a dichromic mirror. A neutral density filter (NDF) was utilized to take part of the SH wave, which was then used to scan the Rb atom saturated absorption spectroscopy (SAS). The setup of the SAS scheme is shown in the dash rounded rectangle of the Fig. 1.

3 Optimization of the experimental parameters

3.1 Optimization of the transmission of the input coupler

One key consideration to improve the SH conversion efficiency of the resonator is the impedance matching of the resonator. For the frequency doubling cavity containing a nonlinear crystal, it means to select the optimum transmission of the input mirror. When the cavity is resonant with the FW, the FW intra-cavity circulating power P_c, FW input power P_1 and SH output power P_2 are expressed as the following equations (Hayasaka et al. 2004; Ou et al. 1992):

$$\frac{P_c}{P_1} = \frac{4T_1}{(T_1 + l + E_{NL}P_c)^2} \tag{1}$$

$$p_2 = T_2 E_{NL} P_C^2 \tag{2}$$

where T_1, l, E_{NL} and T_2 are the transmission of the input coupler (M1), the round-trip linear loss at 1560 nm (excluding T_1), the nonlinear conversion coefficient of MgO:PPLN and the transmission of the output coupler (M4) at 780 nm, respectively. The nonlinear conversion coefficient E_{NL} is measured with a single-pass configuration by removing the input coupler from the cavity. The detailed values are shown in Table 1. In our experiment, the FW was emitted from the PM fiber of the EDFA. The mode matching was optimized via the PM fiber (the scanning cavity results of the FW mode are shown in Fig. 6a), and we removed the "matching term" in the reference of Hayasaka et al. (2004).

To a fixed input FW power, the different transmissions of M1 will lead to different intra-cavity circulating power in the resonator. The optimum transmission of the input coupler depends on the total losses of resonator including linear and nonlinear loss, and it can be described as the following equation (Villa et al. 2007):

$$T_{opt} = \frac{l}{2} + \sqrt{(\frac{l}{2})^2 + \Gamma P_1} \tag{3}$$

where Γ includes all nonlinear losses, and it can be written as the sum of two terms:

$$\Gamma = E_{NL} + \alpha\,(\mathrm{W}^{-1}) \tag{4}$$

where α is the absorption coefficient of nonlinear crystal in the SH process. It is a small quantity in our experiment.

The linear loss l is the crucial parameter used to accurately calculate the optimum transmission of resonators; however, it often brings errors by the direct measurement. In our experiment, instead of direct measuring, we get the $l = 2.54\%$ by fitting the experimental results of SH output power versus FW input power. The detailed fitting processes are shown in Sect. 4. The dependence of the theoretical optimum transmission with the 1560 nm FW input power is shown in Fig. 2. The calculated optimum transmission is $\sim$25.8% to the 5 W FW input power (5 W is the nominal maximum output power of the EDFA).

Table 1 Parameters in the experiment

Parameter	Symbol	Value
Transmission of input coupler at 1560 nm	T_1	25.5% (or 11.0%)
Transmission of output coupler at 780 nm	T_2	99.8%
Radius of curvature of concave mirrors	r	100 mm
Round-trip linear loss of FW	l	2.54%
Cavity length of the resonator	L_{total}	~781 mm
Beam waist spot of FW	ω_{FW}	39 µm
Length of the MgO:PPLN crystal	l_c	25 mm
Nonlinear conversion coefficient of MgO:PPLN	E_{NL}	1.2%/W
Extraordinary refractive index of FW	n_{1560}	2.14
Extraordinary refractive index of SH wave	n_{780}	2.18
Absorption coefficient of FW	α_{1560}	<0.1%/cm
Absorption coefficient of SH wave	α_{780}	<0.1%/cm
Effective nonlinear coefficient of the MgO:PPLN crystal	d_{eff}	14.2 pm/V

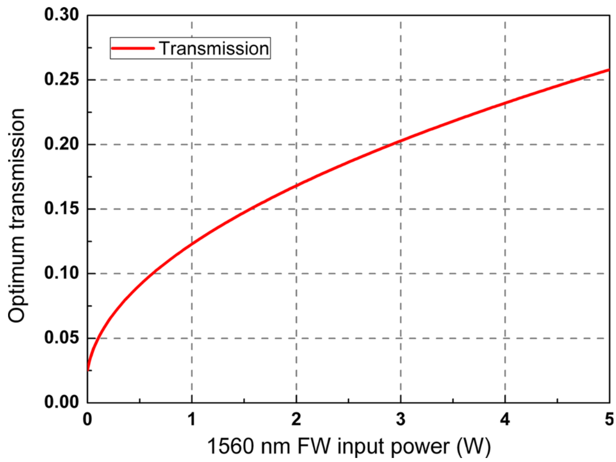

Fig. 2 The dependence of the optimum transmission of the input coupler with the 1560 nm FW input power

3.2 Optimization of the cavity length

A second key consideration to improve the SH conversion efficiency is to achieve the good mode matching of the resonator. There are two steps to reach it. Firstly, to ensure the efficient utilization of the coherent length of the QPM crystal, the cavity waist spot size should be the optimum focus waist spot size. For the given cavity components of the resonator, it means to search for an optimal cavity length design. Secondly, the FW mode volume in the resonator should be a maximum overlap with the optimum cavity mode volume. This step can be given a better performance by using the mode matching lens group instead of the single lens.

The optimum focus waist spot size in the SH parametric process has been given the detailed descriptions by Boyd and Kleinman (1968). To facilitate the narrative, the dimensionless function h called Boyd–Kleinmann (BK) factor was introduced. If the waist spot locates in the middle of the crystal, and the optical wave absorption of the nonlinear crystal can be neglected, the h function will be simplified as:

$$h(\sigma, \beta, \xi) = \frac{1}{4\xi} \int \int_{-\xi}^{\xi} d\tau d\tau' \times \frac{\exp\left[i\sigma(\tau - \tau') - \beta^2 \xi^{-1}(\tau - \tau')\right]}{(1 + i\tau)(1 - i\tau)} \tag{5}$$

There are three independent parameters in the h function: σ, β and ξ. $\sigma = \Delta kb/2$ is the normalized wave vector mismatch. It can be optimized by tuning the crystal temperature in the experiment. The phase-mismatching parameter Δk between two waves is given by

$$\Delta k = 2k_1 - k_2 - 2\pi/\Lambda \tag{6}$$

where k_1 and k_2 are the wave vectors of FW and SH, respectively, and Λ is the grating period of the QPM crystal. $b = k_1\omega^2$ is the FW Gaussian confocal parameter, and ω is the FW waist spot. Additionally, β is the FW double refraction parameter of the crystal. There is no walk-off effect in the QPM crystal and β is 0.

Focusing parameter is written as:

$$\xi = l_c/b \tag{7}$$

Here l_c is the crystal length. It has concluded that the maximum BK factor is $h_{\max} = 1.06$ when $\xi_{\text{opt}} = 2.84$ and $\sigma_{\text{opt}} = 0.57$ (Boyd and Kleinman 1968).

The waist spot size of the resonator can be realized by optimizing cavity length of the resonator. One clear and intuitive procedure of optimization is to plot the cavity length as a function of the cavity waist spot.

Based on round-trip ABCD law of the resonator and the parameters (n_{1560}, l_c and r) in Table 1, the contour plots of round-trip distance L (not contain the distance between M3 and M4) as the function of the cavity waist spot ω and the distance between two concave mirrors L_{M3M4} in the stable region of the resonator are shown in Fig. 3.

According to the BK theory, a higher SH power can be obtained with the optimum waist spot $\omega_{\text{opt}} = 35$ μm, which corresponds to $h_{max} = 1.06$. However, such small waist spot is too sensitive to the distance between the concave mirrors M3 and M4, and it will easily lead the resonator to be an unstable cavity (see Fig. 3). To make clear the influence of the FW waist spot to the SH conversion efficiency, we can calculate the SH output power with different FW waist spots of the resonator.

Based on the sum-frequency generation report of Mimoun et al. (2010), we can deduce the dependence of the nonlinear conversion coefficient E_{NL} with h function in the SH process:

$$E_{NL} = z_1 \frac{4d_{eff}^2 l_c}{(\pi\lambda_{780})^2} h \tag{8}$$

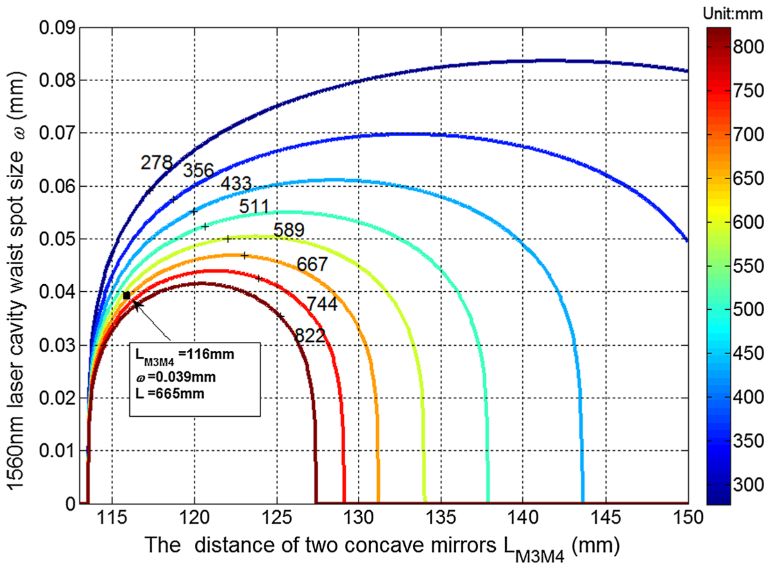

Fig. 3 The contour plots of round-trip distance L (not contain the distance between M3 and M4) as the function of 1560 nm laser cavity waist size ω and the distance between two concave mirrors L_{M3M4} in the stable region of the resonator

where $z_1 = \frac{32\pi\sqrt{\mu_0/\varepsilon_0}}{\lambda_{1560}^2(\frac{2n_{1560}}{\lambda_{1560}} + \frac{n_{780}}{\lambda_{780}})^2}$. The coefficients of d_{eff}, μ_0 and ε_0 are the effective nonlinear coefficient of the MgO:PPLN crystal, the permeability of vacuum and the permittivity of vacuum, respectively. The measured value of d_{eff} to the 5.0% mol. MgO:PPLN crystal was 14.2 pm/V (Gayer et al. 2008). If we substitute Eq. (8) into Eqs. (1) and (2), we can calculate the dependence of the SH output power and the conversion efficiency with different h functions (or the waist spots) at the transmission of T = 25.8%. The calculated results are shown in Fig. 4a, b. The inset shows the details of these curves. The SH output power and the conversion efficiency between the waist size of 39 and 35 μm are very close.

So the final cavity waist spot size we chosen was $\omega_{FW} \sim 39$ μm, corresponding to the parameters of $\xi = 1.87$ and $h = 1.02$. Compared with our previous work, the waist spot size was reduced from 50 to 39 μm (Ge et al. 2015).

To the fixed waist spot size, the concave mirrors distance and the round-trip distance should be determined by two rules. The first is to decrease the astigmatism effects of the concave mirrors M3 and M4 of the cavity. The astigmatism effect of the concave mirrors will reduce the SH conversion efficiency, but the small folding angle of the cavity will be helpful to decrease the astigmatism effects of the concave mirrors. The folding angle should be smaller as possible on the premise that the crystal temperature oven does not block the intra-cavity laser beam. In the meantime, the total cavity length should not be too long. Otherwise, the cavity cannot be locked easily.

The second is the stability of the cavity. Theoretically, when the value of the (A + D)/2 is 0, it will present a good performance of stability of the cavity (A and D are the coefficients of ABCD law). We should choose the cavity design which makes the value of the (A + D)/2 close to 0.

As mentioned above, the concave mirrors distance of 116 mm and the round-trip distance of 665 mm were ultimately determined, corresponding to the folding angle of 7° and the (A + D)/2 of −0.7211.

To achieve a good mode matching of the smaller cavity waist spot, compared with our previous experiment (Ge et al. 2015), the focus lens group (f = 500 mm and f = 300 mm) instead of the single lens was used. The inset of Fig. 6a shows the experimental result of the mode matching.

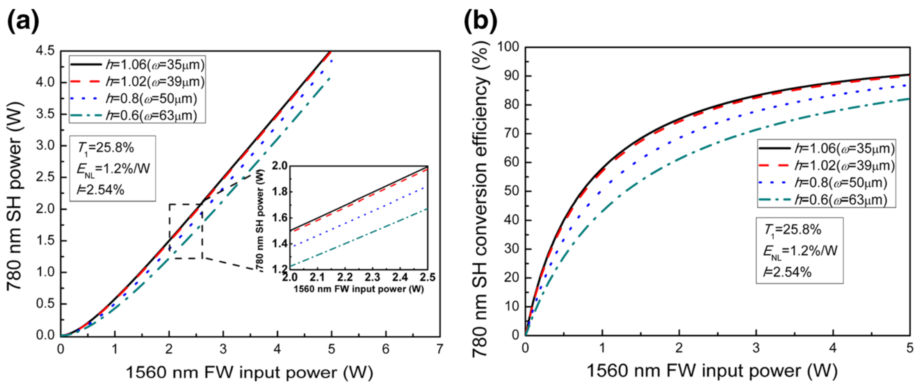

Fig. 4 The dependence of the SH output power (**a**) and conversion efficiency (**b**) with different h functions (or waist spots).The *inset* of (**a**) is the drawing of the partial enlargement

4 SH experimental result and analysis

In order to achieve the optimum normalized wave vector mismatch (σ), the temperature tuning curve of MgO:PPLN was measured. The result is exhibited in Fig. 5. For the purpose of preserving the focusing geometry used in the actual resonant cavity, the temperature tuning curve was obtained by the same configuration as in Fig. 1 but the mirror M1 was removed from the cavity. To avoid unwanted thermal effects, the input FW power was fixed at 500 mW. The phase-matching temperature (PMT) measured is $T_{\mathrm{PM}} = 80.4$ °C for MgO:PPLN with a full width at half-maximum (FWHM) bandwidth of $\Delta\mathrm{T} = 3.5$ °C. The optimum PMT is lower than the PMT exhibited by Ge et al. (2015). The main reason is the more severe thermal effects of the crystal induced by the smaller waist spot used in our experiment (Targat et al. 2005; Han et al. 2014). The thermal effects led to the heating of the MgO:PPLN crystal. As a result, the temperature of the oven had to be lowered to compensate for the rise in crystal temperature, thus resulting in a shift of the phase-matching peak towards lower temperatures (Kumar et al. 2009).

The oscillatory fine structure pattern at the wings was also seen in the temperature tuning curve. The red solid line was fitted by using the $h(\sigma)$ function in Eq. (5) and the formula of the dependence of the single-pass SH output power with the crystal temperature (Boyd and Kleinman 1968), where the phase-mismatch parameter Δk was calculated by the Sellmeier relations (Gayer et al. 2008). The fitted curve presented a good agreement with the experimental data points (including side lobe amplitudes and positions) when the $h(\sigma)$ function was used. The symmetric PMT curve profile implied the good homogeneity of the refractive index of MgO:PPLN crystal (Guo et al. 2014). Additionally, the nonlinear conversion coefficient of $E_{\mathrm{NL}} = 1.2\%/\mathrm{W}$ was also measured with the above single-pass configuration.

As a comparison, two different transmissions of input couplers ($T_1' = 11.0\%$ and $T_1'' = 25.5\%$) were used in the resonator, respectively. The experimental results of the SH output power and conversion efficiency with 1560 nm power are shown in Fig. 6a, b.

The transmission of the input coupler M1 of $T_1' = 11.0\%$ was first to be taken as the input coupler. With the optimum matching temperature of MgO:PPLN and the locked

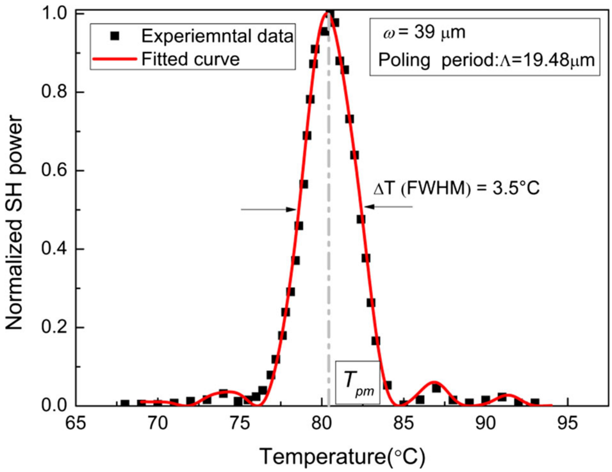

Fig. 5 Measured (*black blocks*) and fitted (*solid line*) temperature tuning curve at $\omega_{\mathrm{FW}} = 39$ μm. (Color figure online)

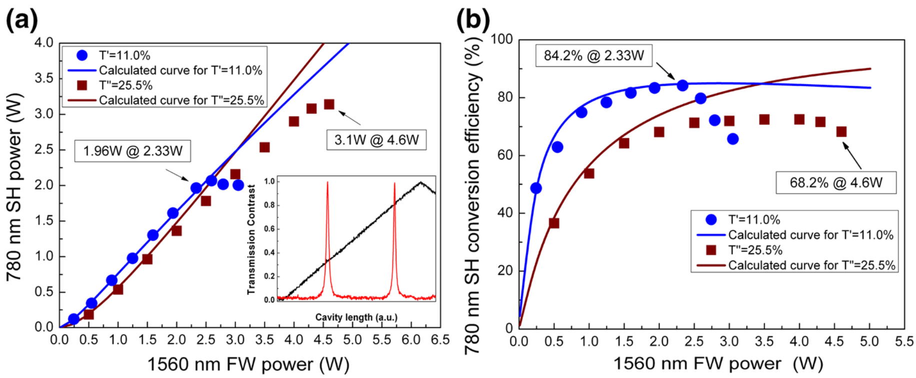

Fig. 6 The SH output power (**a**) and SH conversion efficiency (**b**) versus the mode-matched FW power with input couplings of 11.0% (*blue solid dots*) and 25.5% (*wine solid squares*), respectively. The *inset* of (**a**) is the mode matching result of FW in the scanning cavity. (Color figure online)

cavity length, when the FW power at 1560 nm was 2.33 W, we got an output power of 1.96 W at 780 nm. The maximum SH conversion efficiency was 84.2% (blue solid dots in Fig. 6).

Based on the SH experimental results of the input coupler T_1' and the experimental parameters (T_1', T_2, and E_{NL}), we fitted the linear loss $l = 2.54\%$ by the Eqs. (1) and (2). With the above parameters (l, P_1, and E_{NL}), the optimum transmission of $T_{\mathrm{opt}} \sim 25.8\%$ at the FW power of 5 W was calculated by the Eqs. (3) and (4).

Then a second input coupler with transmission of $T_1'' = 25.5\%$ at 1560 nm was used. Under the identical experimental conditions, we got the maximum SH output power of 3.1 W with the FW input power of 4.6 W, corresponding to a conversion efficiency of 68.2% (wine solid squares in Fig. 6).

The solid lines in Fig. 6 are the calculated curves, which are plotted by the parameters (E_{NL}, l) and the Eqs. (1) and (2). Theoretically, it should be a higher SH conversion efficiency of the resonator with $T_1'' = 25.5\%$ compared with $T_1' = 11.0\%$ at 5 W FW input power level (see the solid line in Fig. 6b). However, the experimental result presented the conflicting results compared with the calculation. The differences between the theoretical and experimental results were mainly caused by the combined effects of the thermal effects of the crystal and the impedance mismatching of the cavity. Compared with the other SH experiments (Hayasaka et al. 2004; Targat et al. 2005; Villa et al. 2007; Feng et al. 2007), the FW input power is higher in our experiment, and the intra-cavity circulating power is even higher. Additionally, the waist spot size was further decreased from 50 to 39 μm in our experiment compared with our previous experiment (Ge et al. 2015). The higher intra-cavity circulating power and the smaller waist spot will both bring severe thermal effects to the crystal. As shown in Fig. 6a, the obvious saturated behaviors of the SH output power exhibited by the two transmissions of the input couplers in the experiment.

The thermal effects will induce the inhomogeneous temperature distribution of the crystal and the shift of the FW focal position (no longer located in the middle of the crystal). These two changes can have detrimental effects on QPM frequency doubling. It is equivalent to the reduction of the nonlinear conversion efficiency E_{NL} (lower than we measured by single-pass configuration in the experiment). The final result is the decreasing of the SH conversion efficiency.

In order to provide a more clear understanding of the thermal effects, we measured the dependence of intra-cavity circulating power of those two input couplers ($T_1' = 11.0\%$ and $T_1'' = 25.5\%$) with the FW input power, respectively. The circulating power in the resonator can be monitored by the power leaking through the cavity mirrors M3 (the reflectivity of M3 is known). The experimental result is given in Fig. 7.

Based on the above experimental results, we can find that the same intra-cavity circulating power ($\sim$13 W) of two transmissions appeared at the FW input power of $\sim$2.5 W. The obvious saturated SH output power of the resonator with $T_1' = 11.0\%$ was also observed near this FW power value (see Fig. 6a). It means that the resonator has already suffered severe thermal effects from this FW input power value.

The maximum SH output power and conversion efficiency with two transmissions are different in different FW input power regions. When the FW input power is lower than 2.5 W, the circulating power of the resonator with $T_1' = 11.0\%$ is higher. It presented the higher SH conversion efficiency and output power of the resonator with $T_1' = 11.0\%$ compared with $T_1'' = 25.5\%$. With the sustained increase of the FW power, the SH output power of the resonator with $T_1' = 11.0\%$ is saturated rapidly due to the thermal effects. When the FW input power is higher than 2.5 W, the circulating power of the resonator with $T_1'' = 25.5\%$ is becoming higher. Due to the more and more severe thermal effects, the SH conversion efficiency of the resonator with $T_1'' = 25.5\%$ is getting lower and lower than the theoretical predictions.

In the meantime, one should note that the saturated behaviors of the SH power are also affected by the impedance mismatching of the cavity. For the transmission lower than the optimum transmission, where the transmission is undercoupled, the output power decreases much faster than it does in the overcoupled region, where the transmission is higher than the optimum transmission (Kaneda and Kubota 1997). According to the calculated result in Fig. 2, the optimum transmission is 18% at the FW power of 2.5 W (This FW power can be called the corresponding impedance matching power of 18%). So the transmission of $T_1' = 11.0\%$ is undercoupled. Combined with the thermal effects, the SH output power corresponding to $T_1' = 11.0\%$ is rapidly saturated at the FW power of $\sim$2.5 W; However,

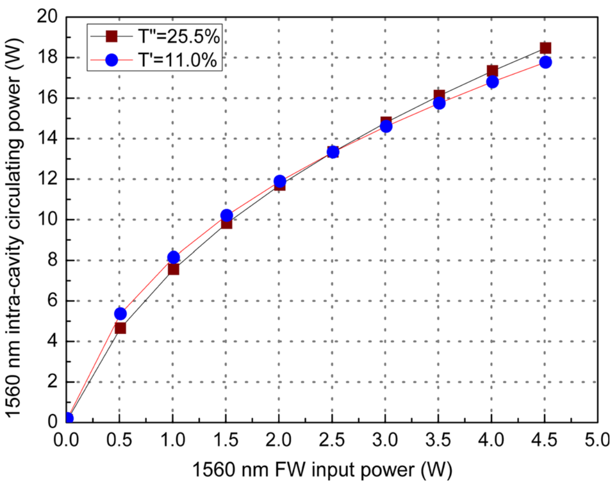

Fig. 7 The dependence of the circulating power of different transmissions of the input couplers with the 1560 nm FW input power

to the transmission of $T_1'' = 25.5\%$, it is overcoupled at the power of 2.5 W. Combined with the thermal effects, the SH output power is gradually saturated when the FW input power is higher than 2.5 W. And it is rapidly saturated when the FW input power is close to the corresponding impedance matching power of $\sim$4.8 W of the $T_1'' = 25.5\%$. The impedance matching power of the $T_1'' = 25.5\%$ can be seen in Fig. 2.

5 Characterization of the SH wave

In a real application, it is an important consideration of SH power stability. The dither-locking method was used to lock the resonator, and a modulation frequency of 13 kHz was applied to the PZT. We monitored the power stability of 780 nm laser by a photo-detector (PED 801-LN, bandwidth 1 MHz). The typical RMS fluctuation of 780 nm output power was 1.29% in 3 h, as seen in Fig. 8. This slight fluctuation of the power is attributed to the slow variation of the FW power and the crystal temperature fluctuation induced by the thermal effects. The power noise of the SH laser can be further suppressed with a mode cleaner (Feng et al. 2008). The longtime SH power stability of the cavity was demonstrated, and it showed the reliability of the dither-locking method.

Continuous frequency tuning is a basic need in many applications (Truong et al. 2013; Baumann et al. 2013; Guo et al. 2013). The SH wave can be frequency tuned by using the PZT that mounted on the mirror M2. When the resonator was locked by the dither-locking method, the SH frequency tuning will follow a slow scanning of the seed ECDL frequency (<0.1 Hz). Taking naturally abundant Rb vapor cell as the frequency ruler, we obtained the saturation absorption spectroscopy (SAS) of ^{87}Rb atom D_2 transition line with the frequency tuning SH laser. The Fig. 9 is a sample scan over the full Doppler-broadened ^{87}Rb D_2 line. The hyperfine structure of ground-state $5S_{1/2}(F_g = 2)$ to excited state $5P_{3/2}$ $(F_e = 1, 2, 3)$ is clearly recognizable. Based on the hyperfine splitting frequency interval, we can infer that 780 nm laser's tunable frequency range is over 2.1 GHz. The further improving of the frequency tuning range is limited by the max on-load voltage of the PZT of the resonator, while the ECDL can be tuned over a 30 GHz range in principle.

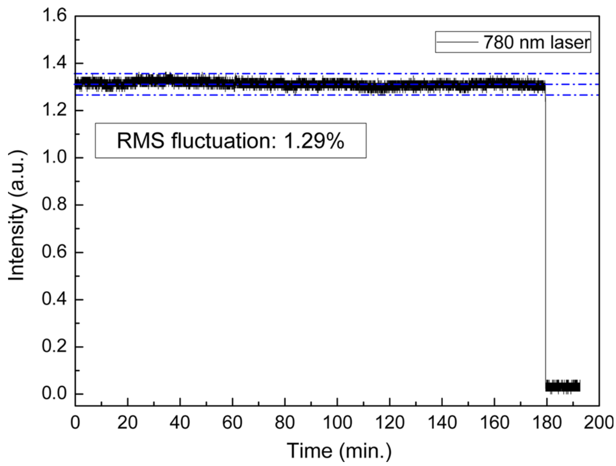

Fig. 8 The measured power stability of 780 nm laser. The typical RMS fluctuation is 1.29% in 3 h

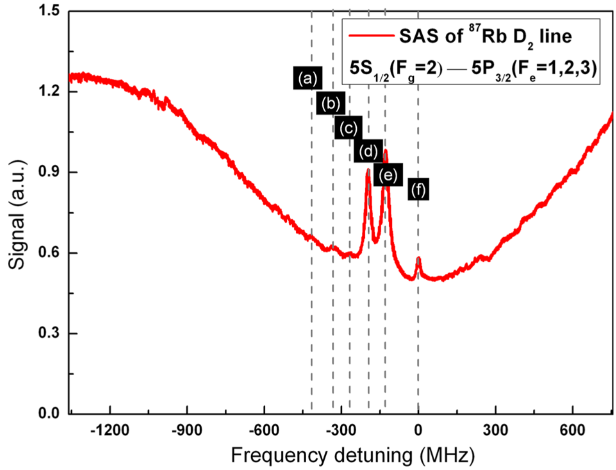

Fig. 9 The SAS of ^{87}Rb atoms by scanning the 780 nm laser frequency. (*a*), $F_g = 2–F_e = 1$; (*b*), $F_g = 2–F_e = 1, 2$; (*c*), $F_g = 2–F_e = 2$; (*d*), $F_g = 2–F_e = 1, 3$; (*e*), $F_g = 2–F_e = 2, 3$; (*f*), $F_g = 2–F_e = 3$

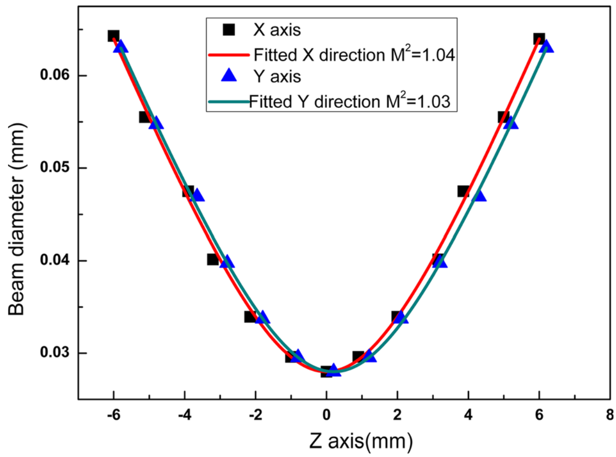

Fig. 10 Beam quality M^2 factor of 780 nm laser for both X and Y axes. The *black solid squares* and *blue solid triangles* are for X axis and Y axis, respectively. The *solid lines* are the fittings for the both axes. (Color figure online)

The generated 780 nm laser beam quality was measured by a "knife edge" method. We measured both X and Y axes of the laser. The M^2 factor is 1.04 and 1.03 for the X and Y axis after being fitted, respectively. The result is shown in Fig. 10.

6 Conclusions

In conclusion, we presented the designs and the performances of a cavity-enhanced frequency-doubled laser source at low pump powers. From two primary considerations of the mode matching and impedance matching, we took a set of optimization measures including the reasonable choice of the cavity waist spot size, the cavity length, the specific distance of the cavity mirrors, the transmission of the input coupler and the using of lens group instead of single lens. Such optimization measures can be helpful to improve the SH power in the cavity-enhanced frequency doubling experiment. The thermal saturated behaviors of the SH output power were both observed with two different transmissions of the input couplers in the experiment. The phenomenon is caused by the combined effects of the thermal effects of the crystal and the impedance mismatching of the resonator. To be convenient to the analysis of the phenomenon, we measured the intra-cavity circulating power of the resonator with these two different transmissions, respectively. The PMT of the MgO:PPLN crystal was fitted by the h function, and the fittings agreed with the experimental data well. When the dither-locking method was used to lock the cavity, the SH wave exhibited the longtime power stability. This method saved the cost of the electro-optic modulator compared with the side-band locking method (Ge et al. 2015). The SH source presented here, with the longtime power stability and the continuous frequency tuning characteristic, can be a potential application in the high-precision atomic spectroscopy and the quantum information process.

Acknowledgements This work is supported by the Doctoral Science Foundation of Taiyuan University of Science and Technology [Grant No. 20162002], the Special Foundation for Theoretical Physics Research Program of China [Grant No. 11647035] and the National Major Scientific Research Program of China [Grant No. 2012CB921601].

References

Ast, S., Nia, R.M., Schönbeck, A., Lastzka, N., Steinlechner, J., Eberle, T., Mehmet, M., Steinlechner, S., Schnabel, R.: High-efficiency frequency doubling of continuous-wave laser light. Opt. Lett. **36**, 3467–3469 (2011)

Baumann, E., Giorgetta, F.R., Coddington, I., Sinclair, L.C., Knabe, K., Swann, W.C., Newbury, N.R.: Comb-calibrated frequency-modulated continuous-wave ladar for absolute distance measurements. Opt. Lett. **38**, 2026–2028 (2013)

Boyd, G.D., Kleinman, D.A.: Parametric interaction of focused Gaussian light beams. J. Appl. Phys. **39**, 3579–3639 (1968)

Chanelière, T., Matsukevich, D.N., Jenkins, S.D., Kennedy, T.A., Chapman, M.S., Kuzmich, A.: Quantum telecommunication based on atomic cascade transitions. Phys. Rev. Lett. **96**, 093604 (2006)

Chiow, S.W., Kovachy, T., Hogan, J.M., Kasevich, M.A.: Generation of 43 W of quasi-continuous 780 nm laser light via high-efficiency, single-pass frequency doubling in periodically poled lithium niobate crystals. Opt. Lett. **37**, 3861–3863 (2012)

Deng, X., Zhang, J., Zhang, Y.C., Li, G., Zhang, T.C.: Generation of blue light at 426 nm by frequency doubling with a monolithic periodically poled $KTiOPO_4$. Opt. Express **21**, 25907–25911 (2013)

Dingjan, J., Darquié, B., Beugnon, J., Jones, M.P.A., Bergamini, S., Messin, G., Browaeys, A., Grangier, P.: A frequency-doubled laser system producing ns pulses for rubidium manipulation. Appl. Phys. B **82**, 47–51 (2006)

Eismann, U., Bergschneider, A., Sievers, F., Kretzschmar, N., Salomon, C., Chevy, F.: 2.1-watts intracavity-frequency-doubled all-solid-state light source at 671 nm for laser cooling of lithium. Opt. Express **21**, 9091–9102 (2013)

Feng, J.X., Li, Y.M., Liu, Q., Liu, J.L., Zhang, K.S.: High-efficiency generation of a continuous-wave single-frequency 780 nm laser by external-cavity frequency doubling. Appl. Opt. **46**, 3593–3596 (2007)

Feng, J.X., Tian, X.T., Li, Y.M., Zhang, K.S.: Generation of a squeezing vacuum at a telecommunication wavelength with periodically poled $LiNbO_3$. Appl. Phys. Lett. **92**, 221102 (2008)

Gayer, O., Sacks, Z., Galun, E., Arie, A.: Temperature and wavelength dependent refractive index equations for MgO-doped congruent and stoichiometric $LiNbO_3$. Appl. Phys. B **91**, 343–348 (2008)

Ge, Y.L., Guo, S.L., Han, Y.S., Wang, J.M.: Realization of 1.5 W 780 nm single-frequency laser by using cavity-enhanced frequency doubling of an EDFA boosted 1560 nm diode laser. Opt. Commun. **334**, 74–78 (2015)

Guo, S.L., Ge, Y.L., Han, Y.S., He, J., Wang, J.M.: Investigation of optical inhomogeneity of MgO:PPLN crystals for frequency doubling of 1560 nm laser. Opt. Commun. **326**, 114–120 (2014)

Guo, S.L., Ge, Y.L., He, J., Wang, J.M.: Singly resonant sum-frequency generation of 520-nm laser via a variable input-coupling transmission cavity. J. Mod. Opt. **62**, 1583–1590 (2015)

Guo, S.L., Wang, J.M., Han, Y.S., He, J.: Frequency doubling of cw 1560 nm laser with single-pass, doubling-pass and cascaded MgO:PPLN crystals and frequency locking to Rb D_2 line. Proc. SPIE **8772**, 87721B (2013)

Guo, X., Zhao, J., Li, Y.: Robust generation of bright two-color entangled optical beams from a phase-insensitive optical parametric amplifier. Appl. Phys. Lett. **100**, 091112 (2012)

Han, Y.S., Wen, X., Bai, J.D., Yang, B.D., Wang, Y.H., He, J., Wang, J.M.: Generation of 130 mW of 397.5 nm tunable laser via ring-cavity enhanced frequency doubling. J. Opt. Soc. Am. B **31**, 1942–1947 (2014)

Hayasaka, K., Zhang, Y., Kasai, K.: Generation of 22.8 mW single-frequency green light by frequency doubling of a 50-mW diode laser. Opt. Express **12**, 3567–3572 (2004)

Henderson, A., Esquinasi, P., Levin, M.: 6.3 Watt single frequency CW source at 780 nm based on frequency conversion of a fiber laser. Proc. SPIE **7582**, 75820F (2010)

Hétet, G., Hosseini, M., Sparkes, B.M., Oblak, D., Lam, P.K., Buchler, B.C.: Photon echoes generated by reversing magnetic field gradients in a rubidium vapor. Opt. Lett. **33**, 2323–2325 (2008)

Hou, F., Xiang, X., Quan, R., Wang, M., Zhai, Y., Wang, S., Liu, T., Zhang, S., Dong, R.: An efficient source of frequency anti-correlated entanglement at telecom wavelength. Appl. Phys. B **122**, 1–8 (2016)

Jensen, O.B., Petersen, P.M.: Generation of single-frequency tunable green light in a coupled ring tapered diode laser cavity. Opt. Express **21**, 6076–6081 (2013)

Kaneda, Y., Kubota, S.: Theoretical treatment, simulation, and experiments of doubly resonant sum-frequency mixing in an external resonator. Appl. Opt. **36**, 7766–7775 (1997)

Khripunov, S., Kobtsev, S., Radnatarov, D.: Efficiency of different methods of extra-cavity second harmonic generation of continuous wave single-frequency radiation. Appl. Opt. **55**, 502–506 (2016)

Khripunov, S., Radnatarov, D., Kobtsev, S., Skorkin, A.: Variable-wavelength second harmonic generation of CW Yb-fibre laser in partially coupled enhancement cavity. Opt. Express **22**, 7046–7051 (2014)

Kobayashi, T., Akamatsu, D., Nishida, Y., Tanabe, T., Yasuda, M., Hong, F.L., Hosaka, K.: Second harmonic generation at 399 nm resonant on the $^1S_0 - {}^1P_1$ transition of ytterbium using a periodically poled $LiNbO_3$ waveguide. Opt. Express **24**, 12142–12150 (2016)

Kumar, S.C., Samanta, G.K., Ebrahim-Zadeh, M.: High-power, single-frequency, continuous-wave second-harmonic-generation of ytterbium fiber laser in PPKTP and MgO: sPPLT. Opt. Express **17**, 13711–13726 (2009)

Li, T., Mitazaki, R., Kasai, K., Okada-Shudo, Y., Watanabe, M., Zhang, Y.: Generation of tripartite quantum correlation among amplitude-squeezed beams by frequency doubling in a singly resonant cavity. Phys. Rev. A **91**, 023833 (2015)

Mimoun, E., Sarlo, L.D., Zondy, J.J., Dalibard, J., Gerbier, F.: Solid-state laser system for laser cooling of sodium. Appl. Phys. B **99**, 31–40 (2010)

Ou, Z.Y., Pereira, S.E., Polzik, E.S., Kimble, H.J.: 85% efficiency for cw frequency doubling from 1.08 to 0.54 um. Opt. Lett. **17**, 640–642 (1992)

Paschotta, R., Kürz, P., Henking, R., Schiller, S., Mlynek, J.: 82% efficient continuous-wave frequency doubling of 1.06 μm with a monolithic $MgO:LiNbO_3$ resonator. Opt. Lett. **19**, 1325–1327 (1994)

Samanta, G.K., Kumar, S.C., Devi, K., Ebrahim-Zadeh, M.: Multicrystal, continuous-wave, single-pass second-harmonic generation with 56% efficiency. Opt. Lett. **35**, 3513–3515 (2010)

Sané, S.S., Bennetts, S., Debs, J.E., Kuhn, C.C.N., McDonald, G.D., Altin, P.A., Close, J.D., Robins, N.P.: 11 W narrow linewidth laser source at 780 nm for laser cooling and manipulation of Rubidium. Opt. Express **20**, 8915–8919 (2012)

Sparkes, B.M., Bernu, J., Hosseini, M., Geng, J., Glorieux, Q., Altin, P.A., Lam, P.K., Robins, N.P., Buchler, B.C.: An ultra-high optical depth cold atomic ensemble for quantum memories. J. Phys: Conf. Ser. **467**, 12009–12013 (2013)

Targat, R.L., Zondy, J.J., Lemonde, P.: 75%-Efficiency blue generation from an intracavity PPKTP frequency doubler. Opt. Commun. **247**, 471–481 (2005)

Thompson, R.J., Tu, M., Aveline, D.C., Lundblad, N., Maleki, L.: High power single frequency 780 nm laser source generated from frequency doubling of a seeded fiber amplifier in a cascade of PPLN crystals. Opt. Express **11**, 1709–1713 (2003)

Truong, G.W., Douglass, K.O., Maxwell, S.E., Zee, R.D., Plusquellic, D.F., Hodges, J.T., Long, D.A.: Frequency-agile, rapid scanning spectroscopy. Nat. Photon. **7**, 532–534 (2013)

Villa, F., Chiummo, A., Giacobino, E., Bramati, A.: High-efficiency blue-light generation with a ring cavity with periodically poled KTP. J. Opt. Soc. Am. B **24**, 576–580 (2007)

Wang, J.M., Zhang, K., Ge, Y.L., Guo, S.L.: Efficient frequency doubler of 1560 nm laser based on a semi-monolithic resonant cavity with a PPKTP crystal. Opt. Commun. **369**, 194–198 (2016)

Wen, X., Han, Y.S., Bai, J.D., He, J., Wang, Y.H., Yang, B.D., Wang, J.M.: Cavity-enhanced frequency doubling from 795 nm to 397.5 nm ultra-violet coherent radiation with PPKTP crystals in the low pump power regime. Opt. Express **22**, 32293–32300 (2014)

Yang, C.S., Xu, S.H., Mo, S.P., Li, C., Feng, Z.M., Chen, D.D., Yang, Z.M., Jiang, Z.H.: 10.9 W kHz-linewidth one-stage all-fiber linearly-polarized MOPA laser at 1560 nm. Opt. Express **21**, 12546–12551 (2013)

Zeil, P., Zukauskas, A., Tjörnhammar, S., Canalias, C., Pasiskevicius, V., Laurell, F.: High-power continuous-wave frequency-doubling in $KTiOAsO_4$. Opt. Express **21**, 30453–30459 (2013)